Label-Free Characterization of Cancer-Activated Fibroblasts Using Infrared Spectroscopic Imaging

S. E. Holton,[†‡] M. J. Walsh,[‡] A. Kajdacsy-Balla,[¶] and R. Bhargava[†‡§*]
[†]Department of Bioengineering, [‡]Beckman Institute for Advanced Science and Technology, and [§]Micro and Nanotechnology Laboratory, University of Illinois at Urbana-Champaign, Urbana, Illinois; and [¶]Department of Pathology, University of Illinois at Chicago, Chicago, Illinois

ABSTRACT Glandular tumors arising in epithelial cells comprise the majority of solid human cancers. Glands are supported by stroma, which is activated in the proximity of a tumor. Activated stroma is often characterized by the molecular expression of α-smooth muscle actin (α-SMA) within fibroblasts. However, the precise spatial and temporal evolution of chemical changes in fibroblasts upon epithelial tumor signaling is poorly understood. Here we report a label-free method to characterize fibroblast changes by using Fourier transform infrared spectroscopic imaging and comparing spectra with α-SMA expression in primary normal human fibroblasts. We recorded the fibroblast activation process by spectroscopic imaging using increasingly tissue-like conditions: 1), stimulation with the growth factor TGFβ1; 2), coculture with MCF-7 human breast cancerous epithelial cells in Transwell coculture; and 3), coculture with MCF-7 in three-dimensional cell culture. Finally, we compared the spectral signatures of stromal transformation with normal and malignant human breast tissue biopsies. The results indicate that this approach reveals temporally complex spectral changes and thus provides a richer assessment than simple molecular imaging based on α-SMA expression. Some changes are conserved across culture conditions and in human tissue, providing a label-free method to monitor stromal transformations.

INTRODUCTION

The stroma is known to play a crucial role in epithelial cancer progression in a variety of tissues (1–4). The stroma has also been suggested as an alternative and potentially more effective therapeutic target to the epithelial tumor itself because the vast heterogeneity in the genomic and histological makeup of epithelial tumors makes individualized treatment expensive and unreliable (5). It is imperative to develop methods to characterize the stroma and hence its transformations in epithelial tumor progression. For example, one hallmark of a cancer-associated stroma is the fibroblast-to-myofibroblast cellular transformation (6). This phenotypic change is characterized by the expression of α-smooth muscle actin (α-SMA), a cytoplasmic protein that increases a cell's contractility and leads to stiffening of the tumor microenvironment (7). The fibroblast-to-myofibroblast transformation has been observed within tumor-adjacent stroma in human tissues (8–10). A similar response can be induced by exposing fibroblasts to elevated levels of transforming growth factor-β1 (TGF-β1) in cell culture (11). Because of this readily observable transition and its effect on the physical properties of the tissue, stromal myofibroblasts have been a focus of research and are important markers in glandular cancers such as breast cancer (10,11). Immunohistochemistry (IHC) is the gold standard for visualizing α-SMA expression in clinical samples, but the use of antibody-based techniques is time-consuming and costly, and it is difficult to quantify protein expression (12). Furthermore, the stromal response is likely more complex than characterized by this single marker. Although considerable advances in immunofluorescence methods have been made (13), only a few known proteins can be simultaneously detected. Even this capability may not be sufficient to catalog the varied cytopathic effects of a multifactorial disease like cancer. Alternative techniques to directly measure cellular transformations in a consistent, quantitative, and multiplexed manner are needed.

As an alternative to molecular imaging, label-free chemical imaging approaches have recently provided reliable correlations between histopathologic status and spectral markers (14–16). Fourier transform infrared (FTIR) spectroscopic imaging, in particular, has been used extensively to study biochemical changes within cells as well as differences between cell lines (17–19). In addition, studies have correlated molecular expression in simple breast cell cultures with spectral properties in both IR (20) and Raman spectroscopy (21). These studies focused on epithelial cells. The fibroblasts' response to epithelial transformations has not been studied in vitro by spectroscopic imaging techniques. Here, we describe a method for characterizing and analyzing the fibroblast-to-myofibroblast transformation. We specifically seek to examine the correlation between the current gold-standard antibody marker and the spectroscopic signature of transformation. We examine transformation in primary normal human dermal fibroblasts (NHDFs) activated with TGFβ1, in cocultures of primary fibroblasts with tumorigenic breast epithelial cells (MCF-7) and human tissues. Although coculture models provide a tissue-like environment, TGFβ1 activation is used as a positive control because it is commonly used in research (7). This comprehensive examination of cells grown in two-dimensional

Submitted March 26, 2011, and accepted for publication July 14, 2011.

*Correspondence: rxb@illinois.edu

Editor: Feng Gai.

0006-3495/11/09/1513/9 $2.00

doi: 10.1016/j.bpj.2011.07.055

(2D) and three-dimensional (3D) cell cultures as well as in human breast tissue will ensure wide research and clinical relevance. However, the presence of other cell types is a potentially confounding analytical factor, and it is not obvious that spectral correlations will hold for mixtures of cell types. Hence, this study is important from the perspective of clinical cancer progression, research in correlating labeled and label-free approaches, and analysis of samples that present a complex bioanalytical background.

MATERIALS AND METHODS

Experimental design

Cell culture models

To observe the effects of cancerous breast epithelium on the surrounding tissue stroma, we used two coculture methods: a Transwell coculture and a 3D cellular coculture model. The Transwell coculture (Fig. 1 *A*) allows for two cell types to communicate via soluble growth factors that diffuse into a shared medium (22). The 3D cellular coculture model (Fig. 1 *B*) consists of cells embedded in a type I collagen hydrogel. Both of these systems are essentially mediated by soluble growth factors; however, cells adhere to a solid substrate in the 2D model and have a different geometry and physical microenvironment. Although 2D monolayer cultures are the staple of cell biology, 3D cultures were recently shown to be a more realistic representation of biological phenomena that occur in tissue (23–28). Hence, an analysis of both systems by means of our approach serves to ensure that the developed method is robust and relevant to different communities of researchers. In addition to these cocultures, we sought to demonstrate that the developed methods are also valid for 2D and 3D cultures of single-cell types. Therefore, we stimulated single-cell-type cultures with TGFβ1 to validate the observed activation.

For 2D cultures, primary NHDFs were grown on MirrIR slides, which allowed for both FTIR transflectance and immunofluorescence imaging. The fibroblasts were cocultured with cancerous breast epithelial cells (MCF-7) or stimulated with TGFβ1. The MCF-7 cells were derived from a human breast tumor that had metastasized to the lung but maintain a cancer stem-cell-like phenotype in culture (29). These cells are less aggressive when injected into nude mice compared with other human breast cancer cell lines, and hence were used in this study as a model of an early cancerous source. Samples were removed from the culture at specific time points (0 h, 6 h, 12 h, and 24 h) and fixed. We analyzed half of the samples using immunofluorescence to detect α-SMA, and spectroscopically imaged the other half. For 3D cultures, samples were prepared as separate layers, with one cell type (NHDF and MCF-7) per layer in a type I collagen matrix. The layers were cocultured for a determined length of time and then separated with forceps. There was no observed cell migration within the time intervals of this experiment, as determined by cell-type-specific expression of cytokeratins for epithelial cells and vimentin for fibroblasts (data not shown). Briefly, the layers were separated, stained according to standard IHC methods, and subsequently imaged with a Zeiss Axiovert 200M (Zeiss, Thornwood, NY). A similar 3D model was previously used to study skin cancer (29). Although the experimental methods employed for both this study and the engineered skin model can be used to study epithelial-fibroblast interactions, the predefined geometry used here allows one to observe molecular changes without morphology-associated effects or changes in the molecular concentration of a growing tumor, which may confound the temporal profile.

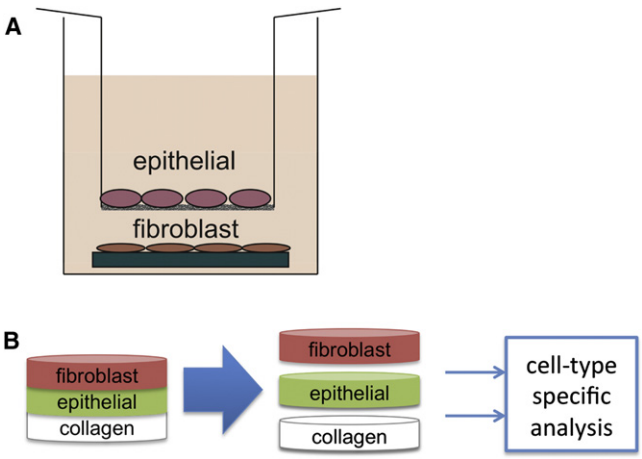

FIGURE 1 (*A*) Schematic of the Transwell coculture system, which allows cells to communicate via soluble growth factors without contact. A filter with a 0.1 μm pore size is used at the bottom of the top basket. (*B*) Schematic of the 3D coculture setup, which is comprised of cells embedded in a type I collagen gel. No membrane separates the layers.

Cell culture

Cell lines and use. Primary adult NHDFs (No. CC-2511; Lonza, Basel, Switzerland) were maintained in fibroblast basal medium supplemented with 0.1% hFGF-B, 0.1% insulin, 0.1% gentamicin/amphotericin-B, and 2% fetal bovine serum (FBS; FGM-2 fibroblast growth medium-2 bullet kit, No. CC3132; Lonza). They were used at passages 8–10 to avoid problems associated with senescence in primary cell lines. The fibroblasts were subcultured according to protocols detailed on the Lonza website, and the Lonza ReagentPack (trypsin/EDTA, trypsin neutralizing solution, HEPES buffered saline solution, No. CC-5034) was used exclusively with this cell type. For serum-free medium, the media were prepared the same way, with the exception that FBS was omitted. MCF-7 (ATCC) cells were maintained in Dulbecco's modified Eagle's essential medium (Invitrogen, Carlsbad, CA) supplemented with 10% FBS (Sigma, St. Louis, MO) and 1% PenStrep (Sigma). They were subcultured according to ATCC protocols every 3 days at 70% confluency.

2D cell culture. Fibroblasts were grown on sterilized MirrIR slides (Kevley Technologies, Chesterland, OH). They were seeded at ~60% confluency and grown for 24 h before being switched to serum-free medium (FGM-2 (Lonza), with additives but not FBS). The samples were grown in serum-free medium for 24 h before coculture. MCF-7 cells were grown on Transwell inserts (0.1 μm pore size; Corning, Corning, NY) in normal growth medium for 24 h and then switched to serum-free medium for an additional 24 h before coculture.

Transwell coculture. The Transwell coculture system is useful for spectroscopy because any IR substrate can be used in the lower chamber of the culture dish (Transwell inserts, 0.1 μm pore, PES; Corning). Pieces of MirrIR Low-E slides were sterilized once with 10% bleach followed by 70% ethanol and left to dry in a sterile biosafety cabinet before use. Immunofluorescence staining was also performed with the MirrIR slides, and there were no detrimental effects on the coated glass surface. The use of MirrIR slides for both immunofluorescence and FTIR measurements ensured that there was no substrate-specific factor that could have induced α-SMA expression independently of soluble growth factors. After 0 h, 6 h, 12 h, and 24 h of coculture, each MirrIR slide was rinsed with sterile 1$\times$ PBS before fixation in 4% paraformaldehyde for 1 h at 4°C. After fixation, the paraformaldehyde was neutralized with 0.1 M glycine for 10 min. Subsequently, the samples were divided: for each time point, two samples were prepared for FTIR imaging and two were prepared for immunofluorescence staining. The samples for FTIR imaging were rinsed with deionized water and left to dry before imaging.

3D cell culture. The cells were maintained as previously described in 2D culture before being suspended in collagen hydrogels (Type I derived from

rat tail; BD Biosciences, Franklin Lakes, NJ). All reagents were kept on ice before plating, because collagen solution will gel slightly at room temperature. In a conical tube on ice, collagen stock solution was diluted to 2 mg/mL with sterile 10× PBS. The cells were trypsinized, centrifuged at 1000 rpm for 3 min, and resuspended in growth medium. After the cells were counted, they were suspended in the collagen solution at a cell density of 420 cells/mL for NHDF and 1.9×10^4 cells/mL for MCF-7. A much lower cell density of fibroblasts than epithelial cells was used because of the tendency of fibroblasts to collapse the hydrogel at high cell density and after activation, and the similarity to fibroblast density in real tissue. Finally, 1 N NaOH was added at 0.023 mL per 1 mL of collagen stock solution to neutralize the acetic acid and allow the collagen to gel. To prepare samples, 200 μL of the collagen and cell suspension were added to each well of a 48-well tissue culture plate. The plates were left at 4°C for 90 min to slow down the polymerization of collagen and obtain a more uniform fiber orientation and width (31). The samples were then placed in a humidified incubator at 37°C for 30 min to polymerize the collagen with cells embedded within. After the samples had gelled, growth medium was added. The cells were allowed to grow for 24 h before being changed to serum-free medium to avoid any confounding effects of growth factors present in FBS. After 48 h in serum-free medium, the coculture layers were stacked together, and 1.5 ng/mL transforming growth factor-β1 (TGFβ1) from human platelets ($\geq$97%, No. T1654; Sigma) in serum-free medium were added to the appropriate fibroblast samples as a positive control. Fresh serum-free medium was added to the cocultured samples. After 0, 6, 12, and 24 h of coculture, the fibroblast layer was fixed in 4% paraformaldehyde overnight before processing for immunofluorescence or FTIR imaging.

3D culture sample preparation. 3D culture samples were paraffin-embedded and sectioned before imaging. First, the paraformaldehyde was gently aspirated from the samples and then the gels were dehydrated by serial ethanol dehydration. The samples were put in 50%, 70%, 80%, and 95% ethanol for 45 min each, followed by three 45-min incubations in 100% ethanol. The samples were then soaked in xylenes for three 45-min periods. Finally, the samples were placed in paraffin in a 60°C oven for two 1-h periods and one 12-h period. The samples were mounted in paraffin blocks and sectioned at 5 μm onto MirrIR slides for FTIR imaging. The samples were deparaffinized in hexanes for 24 h before imaging. For each set of experiments, samples were prepared in duplicate and the experiment was replicated independently to show the reproducibility of both the biological results and absorbance spectra.

Immunofluorescence staining. For immunofluorescence staining, samples were permeabilized in 0.2% TX-100 for 15 min. The samples were washed three times with PBS and then blocked with 1 wt% BSA in PBS/T for 1.5 h. After three washes with PBS/T, the samples were incubated with primary antibody (mouse anti-human α-SMA, 1:100 dilution; Dako, Glostrup, Denmark) overnight at 4°C. The samples were washed again and incubated with secondary antibody (goat anti-mouse IgG-FITC conjugated, 1:80 dilution; Abcam, Cambridge, UK) for 1 h. The samples were mounted with UltraCruz mounting medium for fluorescence with DAPI (No. sc-24941; Santa Cruz Biotechnology, Santa Cruz, CA) and imaged with a Zeiss Axiovert 200M fluorescence microscope. For 3D samples, confocal imaging was performed with a Leica SP2 laser scanning confocal microscope (Leica, Wetzlar, Germany).

Immunohistochemistry. For tissue biopsies, we obtained a tissue microarray (TMA) of 96 1.5-mm human breast tissue cores comprised of normal, epithelial hyperplasia, in situ, benign tumors, and malignant cancer tissues (No. BR961; US Biomax, Rockville, MD). Four serial sections were acquired from the TMA block. One 5-μm-thick tissue section was placed on a BaF_2 substrate for FTIR analyses, and three 5-μm-thick tissue sections were placed on standard glass slides for IHC and hematoxylin and eosin (H&E) staining. IHC staining was performed for vimentin and α-SMA. H&E staining was used for tissue visualization. Staining was performed with the use of a Ventana Benchmark XT automated slide preparation system (Ventana Medical Systems, Tucson, AZ) and Ventana clinical protocols and reagents (XT UltraView DAB protocol;Ventana).

FTIR spectroscopic imaging. FTIR spectroscopic imaging data were recorded with the use of a Perkin Elmer Spotlight 400 imaging system (Perkin Elmer, Waltham, MA). For all cellular samples, both confluent and sparse regions of the sample were imaged in transflection mode, and data from 4000 cm^{-1} to 750 cm^{-1} were saved. A spectral resolution of 8 cm^{-1} was set with 32 scans per pixel averaged to provide higher signal/noise ratio data. An interferometer speed of 1.0 cm/s was used, and a pixel size of 6.25×6.25 μm was used for detection with an MCT linear array. A spectral background was collected on the MirrIR slide using the same parameters but with 120 scans per pixel. Atmospheric correction was performed on the Spotlight instrument, and the files were exported into ENVI-IDL. Images were baseline-corrected and only those pixels with an absorbance > 0.015 a.u. for the peak absorbance at 1656 cm^{-1} (Amide I) were used for further analysis. Spectra were normalized to Amide I to account for variances in cell density.

Absorbance was stronger for the TMA data, and we sought to maintain compatibility with earlier studies on the parameters used. We collected sample data using the same scanning parameters employed for the cell culture samples, with the exceptions of a 4 cm^{-1} resolution with 2 scans per pixel and a mirror speed of 2.2 cm/s. A background was acquired at these parameters with 120 scans averaged. A threshold absorbance of 0.03 a.u. for the 1656 cm^{-1} (Amide I) absorbance peak was employed to determine pixels to be included in the analysis. Regions of interest were manually marked on the absorbance images corresponding to regions of either fibroblast or myofibroblast cells. Cell-type assignations were made based on the IHC staining of the serial tissue sections: fibroblasts stained positive for vimentin and negative for α-SMA, and myofibroblasts stained positive for both vimentin and α-SMA. More than 40,000 pixels corresponding to fibroblasts and >150,000 pixels corresponding to myofibroblasts were identified. From these identified pixels, average spectra were obtained for fibroblast and myofibroblast classes.

RESULTS AND DISCUSSION

The well-characterized fibroblast activation pathway serves as a model system to benchmark spectral (chemical) changes that accompany the phenotypic transformation. We first used the Transwell coculture system to determine whether coculturing normal primary fibroblasts with tumorigenic breast epithelial cells could result in an activated phenotype, as shown previously in fibroblasts isolated from stroma surrounding a tumor in vivo (7) as well as after induction by TGFβ1 in vitro (9). In our coculture with MCF-7 cells, phenotypic changes were induced in the primary dermal fibroblasts within 6 h to the same extent as treatment with 1.5 ng/mL TGFβ1 (Fig. 2). The experiment was repeated for both cases over a time course of 24 h, with time points being taken at 0 (no coculture), 6, 12, and 24 h to observe any potential evolution of this marker over time. The immunofluorescence imaging results showed no visible change in the number of cells expressing α-SMA over time. We did not use any digitally assisted methods to compare intensity levels, because nonspecific fluorescence and photobleaching make it difficult to perform quantitative intensity analyses. Both stimulation with TGFβ1 and coculture with MCF-7 activated fibroblasts within 6 h.

We hypothesized that examining the temporal evolution of IR absorption spectra would yield more information about fibroblast activation than the on-off information derived from immunofluorescence expression of a single

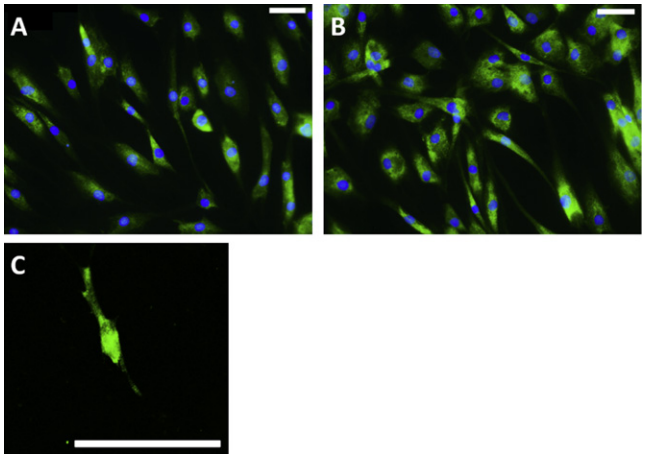

FIGURE 2 After 6 h of stimulation with 1.5 ng/mL TGFβ1 (*A*) or 6 h of coculture with MCF-7 cells (*B*), α-SMA is expressed in dermal fibroblasts. (*C*) Confocal microscopy was used to visualize α-SMA expression in fibroblasts for 3D systems. Scale bar represents 50 μm.

biomarker. Spectra measured from fibroblasts are shown in Fig. 3. Changes were primarily seen in the biomolecular fingerprint region (1800–950 cm^{-1}) and the C-H stretching region (3000–2875 cm^{-1}). In the fingerprint region, larger changes were seen in peaks at 1080 cm^{-1} and 1224 cm^{-1} (Fig. 3, *top*). These are the asymmetric and symmetric vibrational modes of the phosphate bond, which is indicative of changes in nucleic acids. There is an increase in the 1080 cm^{-1} peak, which is usually associated with the symmetric phosphate stretching of DNA. These spectra are averaged to cell density, and the cells were serum-starved before the experiment began, so there should have been little cellular proliferation over the 24 h time course. Serum-starving the cells before coculture arrests them at G0/G1, and this should minimize spectral differences in 1080 cm^{-1} that can be attributed to cells being in different phases of the cell cycle (32–34). The increase at 1080 cm^{-1} indicates that unless there is an increased amount of DNA present in the cells, the assignment of this peak to the phosphate bond of DNA alone may be uncertain. If we account for the total amount of genetic material present within the cell (RNA, DNA, and associated proteins), we may obtain some explanation for the increase in absorbance at this peak. The spectral changes seen could be due to an increase in RNA, changes in chromatin 3D configuration, chromatin sequestration, or an increase in the size of the nucleus. In a recent study, Whelan et al. (35) attributed changes in the 1080 cm^{-1} peak to a transition between native B- and A-like forms of DNA upon dehydration of intact cells. We do not anticipate that the changes seen in these experiments were due to this transition, because all of the samples were fixed and dried completely before spectroscopic imaging was performed.

Between the two treatments (MCF-7 coculture and TGFβ1 stimulation), we observed similar molecular expression of α-SMA but differences in absorption at 1080 cm^{-1}. In the TGFβ1-stimulated samples, the 6- and 12-h samples had an increase in absorption at 1080 cm^{-1} compared with the control, but after 24 h the level had fallen back to the control value. Of interest, at 1224 cm^{-1}, the 6- and 24-h time points were elevated but the 12-h sample had lower absorption than the control. This discrepancy could be the result of the cells being stimulated with TGFβ1 only once at the beginning of the experiment. Thus, the 6-h sample would have a sustained level of TGFβ1 in the medium before the cells were fixed, whereas in the 24-h sample the concentration of TGFβ1 present in the medium would have decreased because it had already been metabolized by the cells. However, in the samples that were cocultured

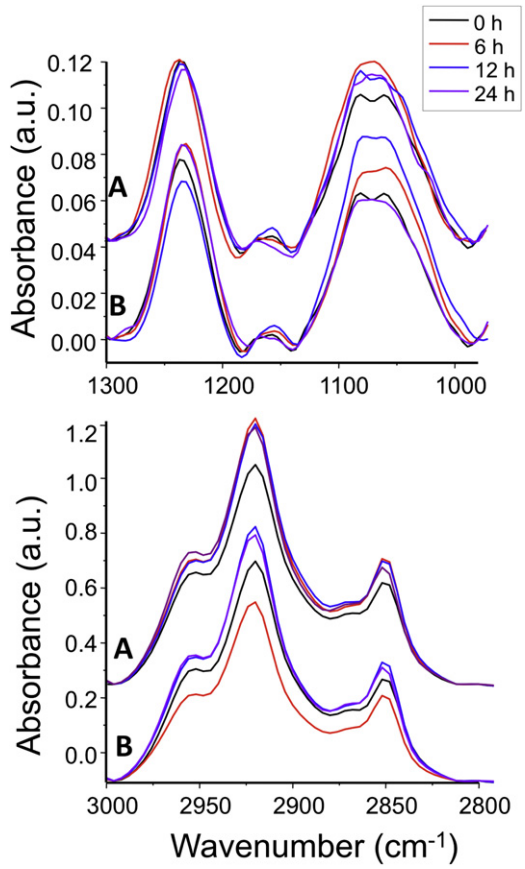

FIGURE 3 Top: In fibroblasts cocultured with MCF-7 (*A*) or stimulated with 1.5 ng/mL TGFβ1 (*B*), normal dermal fibroblasts exhibit changes primarily in the asymmetric and symmetric phosphate stretching bands, indicating bulk changes in the quantity of nucleic acids over time, normalized to 1656 cm^{-1} (Amide I). Fibroblasts activated through coculture show sustained levels of nucleic acids over time, whereas levels wane in the TGFβ1-activated fibroblasts. Bottom: Comparison of the C-H stretching region for fibroblasts cocultured with MCF-7 cells (*A*) or stimulated with TGFβ1 (*B*). Peaks in the C-H stretching region of the spectrum (2960 cm^{-1}, 2932 cm^{-1}, and 2850 cm^{-1}) have a much higher absorbance in the 12- and 24-h time points compared with control. This suggests an increase in cell metabolism resulting from higher amounts of fatty acids. After 6 h of TGFβ1 stimulation, the fibroblasts show lower absorbance in this region compared with control and MCF-7 coculture.

with MCF-7 cells, there was a uniform level of growth factors secreted by the epithelial cells into the shared medium throughout the time course of the experiment. Therefore, we believe that the absorbance at 1224 cm^{-1} may be used as a marker for a sustained fibroblast response to molecular signals released by a malignant epithelium.

In the C-H stretching region, changes were seen in peaks at 2850 cm^{-1}, 2930 cm^{-1}, and 2960 cm^{-1}. This region of the spectrum is correlated with proteins and the carbonyl chains of fatty acids (31). With increasing lengths of time after TGFβ1 stimulation, there was a gradual increase in peak height across all peaks in this region (Fig. 3 *B*, *bottom*). In contrast, coculture with MCF-7 cells yielded a fibroblast response that was more defined, with a very rapid increase in peak height at 2930 cm^{-1} after just 6 h in comparison with the control (Fig. 3 *A*, *bottom*). Although the immunofluorescence results show α-SMA expression in samples stimulated with TGFβ1 or cocultured with MCF-7 cells, the two sets of samples show differences in absorption spectra, permitting a more in-depth biochemical analysis of cellular activation. The reasons for the difference in kinetics of activation likely stem from the coculture providing a host of molecules in the activation pathway via paracrine signaling. Although the mechanisms of the two activations are likely different, this would not be apparent from a single marker. It is also interesting to contrast the ability of spectroscopy to measure transient behavior, which is lacking in the expression of α-SMA. Of course, vibrational spectroscopy does not provide specific protein expression levels in cells. As a general strategy for comprehensive biomolecular analysis, the spectroscopic data can be used to inform the search for appropriate molecular markers by providing the temporal evolution profiles. Further, cellular and subcellular spectral heterogeneity across the sample may occur upon stimulation. These issues have been examined elsewhere (36).

In contrast to the 2D Transwell coculture, culturing cells in a 3D geometry provides an environment that is closer to cellular chemistries in vivo. Cells are known to express surface receptors more faithfully in 3D culture, and are also more likely to differentiate in response to external stimuli (37–39). In the 3D coculture system described here, we used a single cell type and collagen scaffold to fabricate a cylindrical-shaped layer (Fig. 1 *B*). Layers containing different cell types were prepared separately and subsequently stacked on top of each other. This technique allowed for cells to be cocultured by simple stacking. Because the layers are only weakly adherent, they could subsequently be mechanically reseparated for analysis. As described above for the 2D cell culture, we used immunofluorescence staining for α-SMA to probe for the presence of myofibroblasts in 3D by confocal microscopy (Fig. 2 *C*). The immunofluorescence results remained consistent with the Transwell coculture results, i.e., exposure to MCF-7 cells activated fibroblasts along the same time course as TGFβ1 exposure. Another advantage of the 3D cell culture in this setup is that the collagen peaks (1283 cm^{-1}, 1236 cm^{-1}, and 1204 cm^{-1}) can be used for IR spectral analysis, either as a control or to examine microenvironmental changes associated with a growing tumor. These collagen peaks are diagnostically useful for examinations of whole tissue sections (15), and there is evidence that changes in collagen spectra can be detected within a certain distance from a tumor (30,40), which is clinically relevant for cancer pathology. Therefore, we examined the same peaks in the 3D coculture model (Fig. 4 *A*).

The major observation in the three-dimensional coculture model was an overall increase in the absorption of the collagen peaks after coculture with MCF-7 cells over time. This could be a result of fibroblasts locally depositing collagen upon exposure to MCF-7 stimuli. Myofibroblasts play an important role in tissue maintenance, providing a wound-healing-type response by depositing more collagen in the surrounding extracellular matrix (41). TGFβ1 also stimulates fibroblasts to deposit collagen via the Smad pathway, which aids in transcription of the α2(I) procollagen gene, COL1A2 (42). It has been suggested that the fibroblasts present in collagen-dense keloid scars are more susceptible to TGFβ1 (43). Further, the extracellular matrix can act as a control mechanism for the involvement of TGFβ1 in collagen

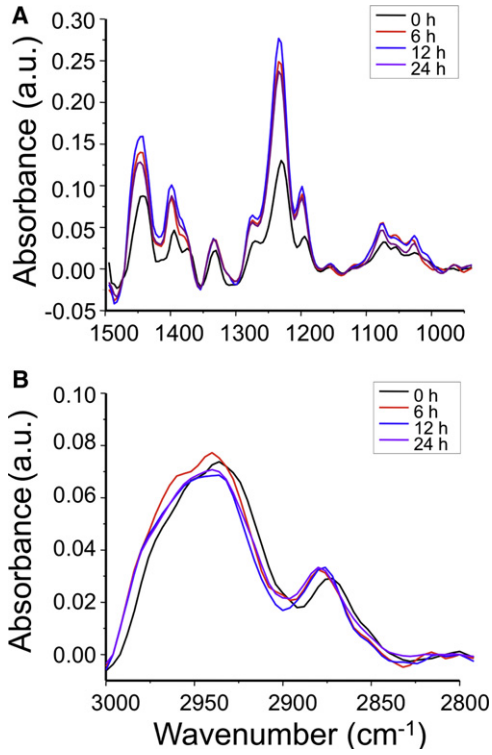

FIGURE 4 (*A*) Characteristic absorbance peaks associated with collagen (1283 cm^{-1}, 1236 cm^{-1}, and 1204 cm^{-1}) are visible and elevated in fibroblasts after coculture with MCF-7. At 1080 cm^{-1} in both 3D and 2D cultures (Fig. 3 *B*), the same cyclical phenomenon is seen. (*B*) The C-H stretching region of the spectrum is distinct from that of the Transwell coculture (Fig. 3 *B, bottom*) spectra.

biosynthesis (44). The other possibility is that upon fibroblast activation, the stiffening of the cells themselves results in contraction of the surrounding gel, making local regions appear more collagen-dense in the absorption spectra. However, no detectable gel contraction was observed upon visual inspection during the time course of this experiment, likely due to the low cell density of fibroblasts embedded within the collagen matrix. For these reasons, we believe that the spectral changes seen in this model are indicative of collagen remodeling by cancer-activated fibroblasts.

Consistent with the 2D culture results, changes were seen in the 1080 cm^{-1} peak in the 3D culture model. There was an increase in this peak initially; however, after 24 h this peak had diminished. The ebb and flow of this nucleic acid signature, even in the environment of persistent epithelial cues, suggests that fibroblasts' molecular expressions settle into a new equilibrium upon an initial exposure to transforming stimuli. This observation is also consistent with changes seen in the Transwell coculture (Fig. 3, *bottom*). There is no change in RNA levels (1224 cm^{-1}) seen in this model compared with the Transwell-culture model. This could be a result of diminished cytoplasmic material from which to record data, because cells appear smaller in the 3D matrix, and thus the cytoplasm is much smaller compared with the nucleus of the cells. Peaks in the C-H stretch region, as with other cultures, may correlate with changes in the phospholipid membrane or protein synthesis after fibroblast activation. Either explanation is plausible considering the physiologic changes that occur during the fibroblast-to-myofibroblast phenotypic change. However, in the 12- and 24-h time points, there is a significant decrease in absorption in this region compared with the control. In general, absorbance in this area was low compared with samples cultured in monolayers, because cells in the 3D cultures were sparsely populated and thinner than those in the 2D cultures. Thus, it is much more challenging to accurately monitor 3D cultures than 2D monolayers. In the C-H stretching region, biochemical changes were dominated by events occurring in the cytoplasm of cells (36), as were the changes at 1224 cm^{-1}. In the 3D culture, as with tissues, it is productive to examine changes due to cellular secretion of growth factors in the surrounding extracellular matrix. However, an examination of changes within the cells themselves requires a subcellular localization of signals, which was not achieved here.

To translate the findings from these studies, we examined clinical breast tissue samples by IR imaging and immunohistochemical staining, including for vimentin and α-SMA. Vimentin (Fig. 5 *B*) will stain for fibroblasts and other mesoderm-derived tissues. In contrast, α-SMA (Fig. 5 *C*) is a protein that is found in myofibroblasts, myoepithelium that lines each gland, and smooth muscle cells that surround blood vessels. Hence, we were able to differentiate between normal and activated fibroblasts by comparing the localization of these two markers in adjacent sections of tissue. In

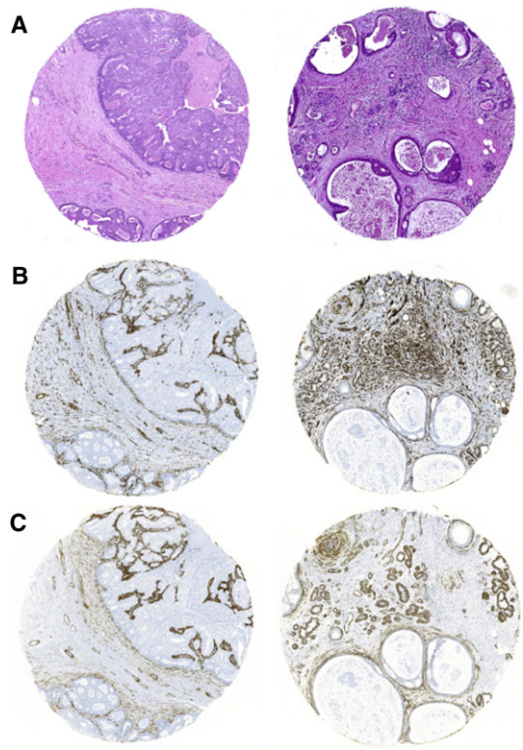

FIGURE 5 Glandular and stromal regions observed in cancerous breast tissue biopsies enable examination of α-SMA expression proximal to cancerous epithelium. (*A*) The morphological features are distinguished by H&E staining. (*B*) Fibroblasts are discerned by IHC staining for vimentin. (*C*) IHC staining for α-SMA is positive for activated fibroblasts (myofibroblasts), myoepithelium (found lining the gland), and smooth muscle (found around blood vessels). α-SMA-positive fibroblasts are located adjacent to the cancerous epithelium, but distal fibroblasts are negative for this protein. Each tissue core (part of a TMA) is 0.5 mm in diameter.

the clinical breast tissue samples, vimentin (in *brown*) is primarily seen in the stroma between glands (Fig. 5 *B*). However, only fibroblasts nearest the cancerous epithelium express α-SMA (Fig. 5 *C*). This is a cancer-associated signature and is diagnostically relevant. To provide a critical comparator with the work performed in our monolayer and 3D coculture models, we examined spectral differences between activated and resting-state fibroblasts in these clinical samples. IR spectroscopic imaging was performed on an entire TMA. Based on the staining of adjacent sections, pixels were manually marked and classified as fibroblast or myofibroblast. The pixels for each class were averaged and these average spectra across the TMA were examined, as shown in Fig. 6. Spectra were compared with the 3D results, because this model should be biologically closest to clinical samples. However, upon examination, the results between the two models are inconsistent. Although the collagen peaks (1300–1050 cm^{-1}) and C-H stretching region (3000–2800 cm^{-1}) are consistent in shape between the 3D culture model and the tissue sample, myofibroblasts from the clinical samples show lower absorbance in the biomolecular fingerprint region (Fig. 6 *A*). Spectra from

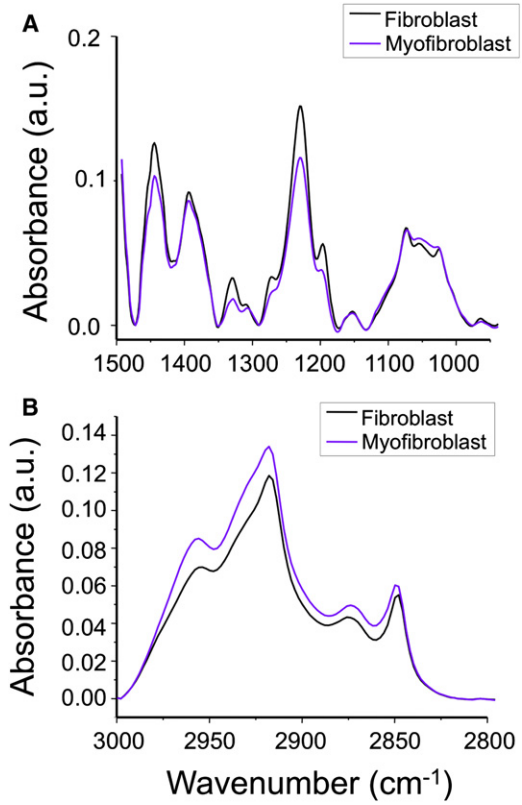

FIGURE 6 Pixels on a TMA were classified as fibroblasts or myofibroblasts based on their average spectra, as shown here. (*A*) Overall normalized absorption was higher for the fibroblast class compared with myofibroblasts. (*B*) However, in the C-H stretching region, myofibroblasts show stronger absorption compared with fibroblasts in the three peaks noted.

the 3D cultures were pure, i.e., they consisted of only normal or activated fibroblasts and type I collagen. The use of clinical samples is invaluable but leads to more variables that become increasingly difficult to control. For example, there is a large degree of variance between patients, even for the noncancerous biopsies (M. J. Walsh, unpublished data). Another interesting issue is whether immunohistochemical stains, used here as the gold standard for comparison, are truly as reliable in clinical samples as in cell culture studies.

Across the three systems described here, activated fibroblasts display spectral changes in the mid-IR regions associated with nucleic acids (1080 cm^{-1}, 1224 cm^{-1}) and C-H stretching modes (2850 cm^{-1}, 2930 cm^{-1}, and 2960 cm^{-1}). Although the 2D and 3D coculture models were mostly consistent, we found some discrepancies between the in vitro and clinical specimens. By studying this transition with FTIR spectroscopy under controlled cell culture conditions, we were able to obtain important information about the potential kinetics of paracrine signaling between epithelial cells and fibroblasts. An investigation of the C-H stretching region of fibroblasts showed an overall increased absorbance at all three peaks across all scenarios, including human breast tissue biopsies (Fig. 6 *B*). The nature of fibroblast activation involves a cellular phenotypic change whereby cytoplasmic proteins are produced and the shape of the cell undergoes a transformation. These biological phenomena can be correlated with the increased absorbance in peaks associated with C-H stretching as a marker for a cancer-activated stromal profile. Because FTIR spectroscopic imaging can be used to study the distribution of chemical changes across the area of a sample, this approach can also be applied to detect early stromal activation in noncancerous areas of a biopsy or tissue resection independently of the expression of a biomarker. This same technique could be expanded to different biological problems, such as testing the effects of drug delivery on distal tissues. By correlating the biological phenomena observed in cell cultures with chemical signatures, we can achieve label-free imaging in complex human tissues.

FTIR spectroscopy and imaging have been employed to measure a wide variety of biomolecular species, including nucleic acids, collagen, glycogen, proteins, and fatty acids. The complex mixtures of these molecules present in cells and tissues implies that IR spectroscopy is useful for determining global biochemical changes in classes of these materials, and is sensitive to the metabolic (45) and local physiologic state of the tissue. In this study, we demonstrate that the method extracts more detailed changes compared with conventional immunofluorescence. The correlations of these changes with mechanistic molecular transitions in the cell can now be established. This next step will link many events in the transformation to a simple, label-free measurement. Because IR imaging data are a convolution of the underlying spectral and structural properties of the tissue (46), the imaging setup (47–49), and optical properties (50–52), it is very challenging to measure specific molecular alterations. Nevertheless, we have shown that some changes in the fibroblast-to-myofibroblast transformation are conserved across monolayer and 3D cultures and human tissues. In summary, IR absorption imaging provides a label-free approach for integrated, first-pass approaches that can yield information about changes in a sample. Such information can provide a basis for studies by itself or an early indication of which biological assays to perform next, and is especially critical for heterogeneous samples in which we need to determine where to perform further molecular analysis.

CONCLUSIONS

In this work, we examined adult NHDFs in monolayer and 3D cell cultures, as well as in formalin-fixed and paraffin-embedded human tissues, to correlate the expression of α-SMA (as observed by immunofluorescence techniques) with chemical changes (as observed by FTIR spectroscopic imaging). Spectral changes were observed predominantly in the C-H stretching region (3290 cm^{-1}) and phosphate bonds

associated with nucleic acids (1224 cm^{-1} and 1080 cm^{-1}). In 3D cocultures and human tissue biopsies, we assessed microenvironmental changes by examining vibrational modes commonly associated with collagen (1283 cm^{-1}, 1236 cm^{-1}, and 1204 cm^{-1}). Fibroblasts activated in vitro via TGFβ1 stimulation or coculture with breast cancer epithelial cells expressed α-SMA and were spectrally distinct from resting-state fibroblast controls. This was also true in the tissue biopsies. However, the spectra from cellular cultures were not entirely consistent with those obtained from tissue, particularly in the phosphate peaks. Although the overall spectral characteristics were conserved between the 3D culture and biopsies, specific absorbance values were inconsistent. Furthermore, there was a spatial dependence of this expression based on the distance of the fibroblasts from the tumor source, as determined by analysis of the collagen peaks and expression of α-SMA in tissue. By directly extracting the spectral signatures of fibroblast activation, the analysis presented here can potentially provide new information, be conducted in a high-throughput manner, and reduce variability, time, and costs. Finally, this work represents a novel (to our knowledge) use of IR spectroscopic imaging to examine stromal changes associated with tumor progression.

SUPPORTING MATERIAL

Tables containing average absorbance values and statistics for all trials are available at http://www.biophysj.org/biophysj/supplemental/S0006-3495(11)00954-4.

This study was supported by the Komen for the Cure Foundation (KG081426), the Prostate Cancer Research Program of the Department of Defense (W81XWH-07-1-0242), and the National Institutes of Health (R01CA138882). S.E.H. received support from the Midwest Cancer Nanotechnology Training Center, NIH National Cancer Institute Alliance for Nanotechnology in Cancer (grant R25 CA154015A).

REFERENCES

1. Illmensee, K., and B. Mintz. 1976. Totipotency and normal differentiation of single teratocarcinoma cells cloned by injection into blastocysts. *Proc. Natl. Acad. Sci. USA.* 73:549–553.
2. Atula, S., R. Grenman, and S. Syrjänen. 1997. Fibroblasts can modulate the phenotype of malignant epithelial cells in vitro. *Exp. Cell Res.* 235:180–187.
3. Weaver, V. M., O. W. Petersen, …, M. J. Bissell. 1997. Reversion of the malignant phenotype of human breast cells in three-dimensional culture and in vivo by integrin blocking antibodies. *J. Cell Biol.* 137:231–245.
4. Dolberg, D. S., and M. J. Bissell. 1984. Inability of Rous sarcoma virus to cause sarcomas in the avian embryo. *Nature.* 309:552–556.
5. Ingber, D. E. 2008. Can cancer be reversed by engineering the tumor microenvironment? *Semin. Cancer Biol.* 18:356–364.
6. Barcellos-Hoff, M. H., and D. Medina. 2005. New highlights on stroma-epithelial interactions in breast cancer. *Breast Cancer Res.* 7:33–36.
7. Rønnov-Jessen, L. 1996. Stromal reaction to invasive cancer: the cellular origin of the myofibroblast and implications for tumor development. *Breast J.* 2:320–339.
8. Bhowmick, N. A., E. G. Neilson, and H. L. Moses. 2004. Stromal fibroblasts in cancer initiation and progression. *Nature.* 432:332–337.
9. Hawsawi, N. M., H. Ghebeh, …, A. Aboussekhra. 2008. Breast carcinoma-associated fibroblasts and their counterparts display neoplastic-specific changes. *Cancer Res.* 68:2717–2725.
10. Bauer, M., G. Su, …, A. Friedl. 2010. Heterogeneity of gene expression in stromal fibroblasts of human breast carcinomas and normal breast. *Oncogene.* 29:1732–1740.
11. Rønnov-Jessen, L., O. W. Petersen, …, M. J. Bissell. 1995. The origin of the myofibroblasts in breast cancer. Recapitulation of tumor environment in culture unravels diversity and implicates converted fibroblasts and recruited smooth muscle cells. *J. Clin. Invest.* 95:859–873.
12. Camp, R. L., G. G. Chung, and D. L. Rimm. 2002. Automated subcellular localization and quantification of protein expression in tissue microarrays. *Nat. Med.* 8:1323–1327.
13. Giltnane, J. M., J. R. Murren, …, B. L. King. 2006. AQUA and FISH analysis of HER-2/neu expression and amplification in a small cell lung carcinoma tissue microarray. *Histopathology.* 49:161–169.
14. Diem, M., P. Griffiths, and J. Chalmers. 2008. Vibrational Techniques in Medical Diagnostics. Wiley, New York.
15. Fernandez, D. C., R. Bhargava, …, I. W. Levin. 2005. Infrared spectroscopic imaging for histopathologic recognition. *Nat. Biotechnol.* 23: 469–474.
16. German, M. J., A. Hammiche, …, F. L. Martin. 2006. Infrared spectroscopy with multivariate analysis potentially facilitates the segregation of different types of prostate cell. *Biophys. J.* 90:3783–3795.
17. Zhang, L., G. W. Small, …, E. N. Lewis. 2003. Classification of Fourier transform infrared microscopic imaging data of human breast cells by cluster analysis and artificial neural networks. *Appl. Spectrosc.* 57:14–22.
18. Bogomolny, E., M. Huleihel, …, S. Mordechai. 2007. Early spectral changes of cellular malignant transformation using Fourier transform infrared microspectroscopy. *J. Biomed. Opt.* 12:024003.
19. Diem, M., C. Matthäus, …, N. Laver. 2009. Infrared and Raman spectroscopy and spectroscopic imaging of individual cells. *In* Infrared and Raman Spectroscopic Imaging. R. Salzer and H. W. Siesler, editors. Wiley-VCH, Weinheim. 173–188.
20. Yang, W., X. Xiao, …, Q. Cai. 2009. In situ evaluation of breast cancer cell growth with 3D ATR-FTIR spectroscopy. *Vib. Spectrosc.* 49:64–67.
21. Hartsuiker, L., N. J. L. Zeijen, …, C. Otto. 2010. A comparison of breast cancer tumor cells with varying expression of the Her2/neu receptor by Raman microspectroscopic imaging. *Analyst (Lond.).* 135:3220–3226.
22. Rozenchan, P. B., D. M. Carraro, …, M. M. Brentani. 2009. Reciprocal changes in gene expression profiles of cocultured breast epithelial cells and primary fibroblasts. *Int. J. Cancer.* 125:2767–2777.
23. Tibbitt, M. W., and K. S. Anseth. 2009. Hydrogels as extracellular matrix mimics for 3D cell culture. *Biotechnol. Bioeng.* 103:655–663.
24. Yamada, K. M., and E. Cukierman. 2007. Modeling tissue morphogenesis and cancer in 3D. *Cell.* 130:601–610.
25. Martin, K. J., D. R. Patrick, …, M. V. Fournier. 2008. Prognostic breast cancer signature identified from 3D culture model accurately predicts clinical outcome across independent datasets. *PLoS ONE.* 3:e2994.
26. Liu, V. A., and S. N. Bhatia. 2002. Three-dimensional photopatterning of hydrogels containing living cells. *Biomed. Microdevices.* 4:257–266.
27. Nelson, C. M., J. L. Inman, and M. J. Bissell. 2008. Three-dimensional lithographically defined organotypic tissue arrays for quantitative analysis of morphogenesis and neoplastic progression. *Nat. Protoc.* 3:674–678.
28. Pampaloni, F., E. G. Reynaud, and E. H. K. Stelzer. 2007. The third dimension bridges the gap between cell culture and live tissue. *Nat. Rev. Mol. Cell Biol.* 8:839–845.
29. Mackenzie, I. C. 2006. Stem cell properties and epithelial malignancies. *Eur. J. Cancer.* 42:1204–1212.

30. Kong, R., R. K. Reddy, and R. Bhargava. 2010. Characterization of tumor progression in engineered tissue using infrared spectroscopic imaging. *Analyst (Lond.).* 135:1569–1578.

31. Sung, K. E., G. Su, …, D. J. Beebe. 2009. Control of 3-dimensional collagen matrix polymerization for reproducible human mammary fibroblast cell culture in microfluidic devices. *Biomaterials.* 30:4833–4841.

32. Holman, H. Y., M. C. Martin, …, W. R. McKinney. 2000. IR spectroscopic characteristics of cell cycle and cell death probed by synchrotron radiation based Fourier transform IR spectromicroscopy. *Biopolymers.* 57:329–335.

33. Hammiche, A., M. J. German, …, F. L. Martin. 2005. Monitoring cell cycle distributions in MCF-7 cells using near-field photothermal microspectroscopy. *Biophys. J.* 88:3699–3706.

34. Flower, K. R., I. Khalifa, …, P. Gardner. 2011. Synchrotron FTIR analysis of drug treated ovarian A2780 cells: an ability to differentiate cell response to different drugs? *Analyst (Lond.).* 136:498–507.

35. Whelan, D. R., K. R. Bambery, …, B. R. Wood. 2011. Monitoring the reversible B to A-like transition of DNA in eukaryotic cells using Fourier transform infrared spectroscopy. *Nucleic Acids Res.* 39:5439–5448.

36. Holton, S. E., M. J. Walsh, and R. Bhargava. 2011. Subcellular localization of early biochemical transformations in cancer-activated fibroblasts using infrared spectroscopic imaging. *Analyst (Lond.).* 136:2953–2958.

37. Menendez, J. A., and R. Lupu. 2007. Fatty acid synthase and the lipogenic phenotype in cancer pathogenesis. *Nat. Rev. Cancer.* 7:763–777.

38. Albrecht, D. R., G. H. Underhill, …, S. N. Bhatia. 2006. Probing the role of multicellular organization in three-dimensional microenvironments. *Nat. Methods.* 3:369–375.

39. Cukierman, E., R. Pankov, and K. M. Yamada. 2002. Cell interactions with three-dimensional matrices. *Curr. Opin. Cell Biol.* 14:633–639.

40. Dhimolea, E., M. V. Maffini, …, C. Sonnenschein. 2010. The role of collagen reorganization on mammary epithelial morphogenesis in a 3D culture model. *Biomaterials.* 31:3622–3630.

41. Desmoulière, A., C. Guyot, and G. Gabbiani. 2004. The stroma reaction myofibroblast: a key player in the control of tumor cell behavior. *Int. J. Dev. Biol.* 48:509–517.

42. Chen, S. J., W. Yuan, …, J. Varga. 1999. Stimulation of type I collagen transcription in human skin fibroblasts by TGF-β: involvement of Smad 3. *J. Invest. Dermatol.* 112:49–57.

43. Bettinger, D. A., D. R. Yager, …, I. K. Cohen. 1996. The effect of TGF-β on keloid fibroblast proliferation and collagen synthesis. *Plast. Reconstr. Surg.* 98:827–833.

44. Streuli, C. H., C. Schmidhauser, …, R. Derynck. 1993. Extracellular matrix regulates expression of the TGF-β 1 gene. *J. Cell Biol.* 120:253–260.

45. Ellis, D. I., and R. Goodacre. 2006. Metabolic fingerprinting in disease diagnosis: biomedical applications of infrared and Raman spectroscopy. *Analyst (Lond.).* 131:875–885.

46. Bhargava, R. 2007. Towards a practical Fourier transform infrared chemical imaging protocol for cancer histopathology. *Anal. Bioanal. Chem.* 389:1155–1169.

47. Levin, I. W., and R. Bhargava. 2005. Fourier transform infrared vibrational spectroscopic imaging: integrating microscopy and molecular recognition. *Annu. Rev. Phys. Chem.* 56:429–474.

48. Diem, M., M. Romeo, …, C. Matthaus. 2004. A decade of vibrational micro-spectroscopy of human cells and tissue (1994-2004). *Analyst (Lond.).* 129:880–885.

49. Baker, M. J., E. Gazi, …, P. Gardner. 2009. Investigating FTIR based histopathology for the diagnosis of prostate cancer. *J Biophotonics.* 2:104–113.

50. Davis, B. J., S. Carney, and R. Bhargava. 2010. Theory of infrared microspectroscopy for intact fibers. *Anal. Chem.* 83: 525–32.

51. Tseng, S. H., A. Grant, and A. J. Durkin. 2008. In vivo determination of skin near-infrared optical properties using diffuse optical spectroscopy. *J. Biomed. Opt.* 13:014016.

52. Cuccia, D. J., F. Bevilacqua, …, B. J. Tromberg. 2009. Quantitation and mapping of tissue optical properties using modulated imaging. *J. Biomed. Opt.* 14:024012.